Enhanced antimicrobial, antibiofilm and ecotoxic activities of nanoencapsulated carvacrol and thymol as compared to their free counterparts

Jina Yammine, Adem Gharsallaoui, Alexandre Fadel, Samah Mechmechani, Layal Karam, Ali Ismail, Nour-Eddine Chihib

Biofilm 4 (2022) 100094

Contents lists available at ScienceDirect

Biofilm

journal homepage: www.sciencedirect.com/journal/biofilm

Dynamic *Salmonella* Enteritidis biofilms development under different flow conditions and their removal using nanoencapsulated thymol

Jina Yammine [a,b], Adem Gharsallaoui [c], Layal Karam [d], Ali Ismail [b], Alexandre Fadel [e], Nour-Eddine Chihib [a,*]

[a] Univ Lille, CNRS, INRAE, Centrale Lille, UMR 8207 – UMET – Unité Matériaux et Transformations, Lille, France
[b] Plateforme de Recherches et d'Analyses en Sciences de l'Environnement (PRASE), Ecole Doctorale des Sciences et Technologies, Université Libanaise, Hadath, Lebanon
[c] Univ Lyon, Université Claude Bernard Lyon 1, CNRS, LAGEPP UMR, 5007, Villeurbanne, France
[d] Human Nutrition Department, College of Health Sciences, QU Health, Qatar University, Doha, Qatar
[e] Univ Lille, CNRS, INRAE, ENSCL, Université d'Artois, FR 2638 – IMEC – Institut Michel-Eugène Chevreul, F-59000, Lille, France

ARTICLE INFO

Keywords:
Dynamic biofilm
Hydrodynamic conditions
Nanoencapsulation
Salmonella enteritidis
Disinfection
Thymol

ABSTRACT

In food industries, microbial contaminations are difficult to control due to the recurrent formation of biofilms that hinders antimicrobials penetration and efficiency. An understanding of Salmonella Enteritidis biofilms behavior under flow conditions is a key to develop efficient preventive and control strategies. S. Enteritidis biofilms displayed 5.96, 6.28 and 6.80 log CFU cm^{-2} under 0.006 cm s^{-1}, 0.045 cm s^{-1}, and 0.087 cm s^{-1} flow velocities, respectively. Biofilms exposed to higher nutrient conditions under greater flow rates, induced significantly more biofilm biomass. To control biofilms, the disinfection efficiency of thymol (THY) was assessed under dynamic conditions by encapsulation it into two types of nanocapsules: monolayer (ML) nanocapsules prepared with a single carrier material (maltodextrin), and layer-by-layer (LBL) nanocapsules prepared by combining two carrier materials (maltodextrin and pectin). A combined mixture of ML and LBL nanocapsules at ½ their minimal inhibitory concentrations induced 99.99% eradication of biofilms developed under the highest flow conditions, after 5 h. ML nanocapsules decreased significantly bacterial counts during the first 0.5 h, while LBL nanocapsules eliminated the remaining bacterial cells and ensured a protection from bacterial contamination for up to 5 h by releasing THY in a sustained manner over time due to the thicker shell wall structure.

1. Introduction

In agro-food processing plants, persistent contamination of surfaces by spoilage or pathogenic microorganisms with their subsequent biofilm formation causes serious health concerns [1,2]. Eighty percent of microbial infections has been associated with food-borne pathogens in a biofilm state [3,4]. Thereby, biofilms are considered a real threat to food industries in terms of compromised products quality and decreased shelf-life. Moreover, biofilms may cause cross-contamination, increased possibility of foodborne diseases and outbreaks, deterioration of equipment due to corrosion, reduced heat transfer and mechanical blockage, coupled with costly significant economic losses [4–7]. *Salmonella* Enteritidis is involved in up to 85% of foodborne outbreaks in Europe with more than €3 billion of annual expenses [8]. *S.* Enteritidis has shown the ability to form biofilms due to their appendages as flagella that allow their adhesion to surfaces with an increased resistance to antimicrobial agents [9,10]. Therefore, increased efforts are urgently needed to control *S.* Enteritidis biofilms that represent a continuous source of contamination and threat to human health. In food industries, biofilms may encounter a wide range of hydrodynamic conditions as in pipelines, tubes, tanks, etc.., and especially during the operating cycles and the clean-in-place (CIP) procedures. These dynamic conditions can strongly affect the morphology, physiology, as well as the formation and detachment of biofilms from surfaces [11–13].

Classical cleaning and disinfection strategies have shown decreased efficiency towards biofilms removal due to the increased microbial resistance, in addition to the reduced diffusion owing to the extrapolymeric matrix that acts as a protective barrier for biofilms [1,6,14]. Therefore, alternative strategies such as the use of nano-based delivery systems encapsulating biosourced terpenes from essential oils (EOs) such as thymol (THY) have aroused as impressive control strategies with remarkable antibiofilm effectiveness against a wide range of pathogenic

* Corresponding author. Certia Inrae, 369 rue Jules Guesde, 59650, Villeneuve d'Ascq, France.
E-mail address: nour-eddine.chihib@univ-lille.fr (N.-E. Chihib).

https://doi.org/10.1016/j.bioflm.2022.100094
Received 9 August 2022; Received in revised form 8 November 2022; Accepted 9 November 2022
Available online 26 November 2022

microorganisms [5,7,15–17]. THY is recognized as safe to be used in food industries by the Food and Drug Administration (FDA) [18,19]. Its encapsulation could be a promising tool to overcome the different obstacles arising not only from free terpenes as their high volatility and low stability but also from the biofilm structures barriers and their resistance mechanisms to microorganisms [12,20].

Accordingly, the purpose of this study was to investigate the effect of different dynamic conditions on the formation of *S*. Enteritidis biofilms in a lab-scale pipeline system. Moreover, the disinfection efficiency of monolayer (ML) and layer-by-layer (LBL) THY nanocapsules was investigated on the highest biofilm biomass reported. ML nanocapsules were prepared using maltodextrins as carrier materials and sodium caseinate as emulsifier, while for the LBL nanocapsules, an additional pectin interfacial layer was added. To mimic the industrial cleaning procedures at a lab-scale, the nanocapsules antimicrobial activity was assessed dynamically on biofilms developed in the pipelines.

2. Materials and methods

2.1. Bacterial strains and culture conditions

S. Enteritidis was selected for this study due to its ability to form highly resistant biofilms to the conventional cleaning and disinfection procedures on both abiotic and biotic surfaces [3]. One hundred μL of overnight precultures of *S.* Enteritidis (CIP 8297) were inoculated into 50 mL of Tryptic Soy Broth (TSB; Biokar Diagnostics, Pantin, France) and incubated at 37 °C until the achievement of the mid-exponential phase. Bacterial cells were then harvested by centrifugation at 5000 rpm for 5 min at 25 °C and washed twice with Potassium Phosphate Buffer (PPB; 100 mM, pH 7).

2.2. Chemicals and antimicrobials

THY (≥99% purity) was purchased from Sigma-Aldrich (St. Louis, MO, USA). For the preparation of the nanocapsules, sodium caseinate (CAS; Fisher Scientific, United Kingdom) was used as emulsifier, low methoxyl pectin (LMP; Cargill, Baupte, France) as additional interfacial layer, and maltodextrins DE 21 (MD; Roquette-Frères SA, Lestrem, France) were used as carrier materials. Sodium hydroxide (NaOH; Sigma-Aldrich, France) and a pure alkaline foaming liquid detergent (RBS-T105; Traitements Chimiques de Surfaces, France) were used for the cleaning of the pipelines and fittings between trials.

2.3. Biofilm formation

2.3.1. Preparation of stainless steel coupons, pipes, fittings and plastic tubes

Stainless steel (SS) (INOX 304 L, Equinox, France) material was chosen for this study as it is easy to clean, chemically inert, extremely resistant to corrosion at a wide range of processing temperatures, and is widely used in food industries [4]. Rectangular SS coupons of 14 mm width, 44 mm length and 1 mm thickness, and pipes of 14 mm inner width, 220 mm length and 5 mm inner height were used for biofilm formation. Prior to each experiment, coupons, pipes and fittings were sanitized by washing with ethanol (Fluka, Sigma-Aldrich, France), then properly rinsed with distilled water and immersed in a neutral detergent for 15 min. They were then thoroughly rinsed with distilled water and dried in a heat oven for 1 h at 180 °C. Plastic tubes (6 × 9 mm, Saint-Gobain Performance Plastics, France) were also sterilized at 121 °C for 20 min. Material were then placed in sterile conditions until being used for the formation of dynamic biofilms.

2.3.2. Dynamic conditions

The set up to form biofilms in SS pipelines under different dynamic conditions is schematically represented in Fig. 1. For each experimental set up, a set of three pipes was used. Five SS coupons were placed horizontally in the inner surface of each pipe. To assess the difference in biofilm biomass formation, three different flow velocities of 0.006 cm s^{-1}, 0.045 cm s^{-1} and 0.087 cm s^{-1} were generated and applied. For each independent experiment, the flow velocity in pipes was maintained constant using a peristaltic pump (Coler-Parmer Instrument CO., Chicago, IL. 60648, U.S.A.). Then for biofilm formation, a 10^7 CFU mL^{-1} *S.* Enteritidis suspension was circulated continuously in the pipes in a closed circuit for 1 h to allow bacterial adhesion. Pipes were then drained, and a PPB solution was circulated to remove non-adherent cells. The whole set up was incubated at 37 °C for 24 h with TSB solution being pumped peristaltically into the pipes in a closed circuit to allow biofilm formation. After overnight incubation, the TSB solution was drained and the pipes were rinsed with a circulating PPB solution. Out of the five coupons installed in each pipe, only the three central coupons were removed and subjected to the different treatments and to the microscopic observations described below.

2.4. Assessment of biofilm formation under different dynamic conditions

2.4.1. Biofilm enumeration

To quantify biofilms developed on SS coupons under the different flow conditions, adhered bacterial cells were detached by immersing coupons into 20 mL of Tryptone Salt Broth (TS; Biokar Diagnostics, France) followed by a vortex for 30 s, a sonication for 5 min (37 kHz; Elmasonic S60H, Elma, Germany) and a subsequent vortex for 30 s. Detached cells were serially dilution in TS broth and plated on Tryptic Soy Agar (TSA; Biokar Diagnostics, France). Culturable cell counting was performed after 24 h incubation at 37 °C. Results were expressed as log CFU cm^{-2}. Three independent experiments were performed for each condition.

2.4.2. Epifluorescence microscopy

The structure and spatial distribution of dynamic biofilms developed

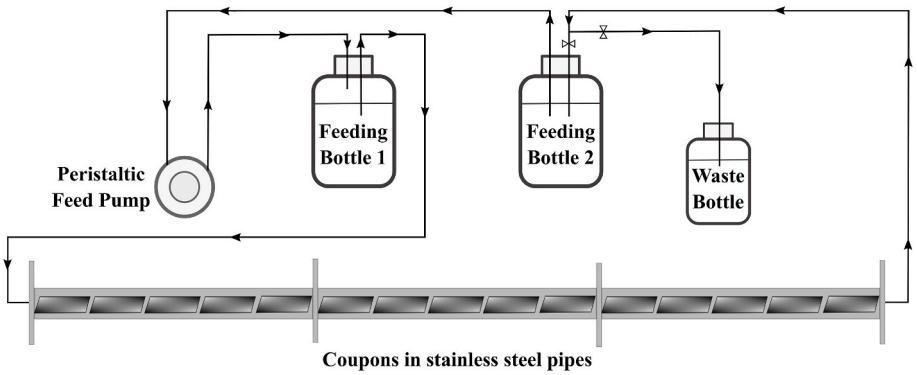

Fig. 1. Schematic representation of the set-up used for dynamic biofilm formation.

on SS coupons were observed under the epifluorescence microscopy (Olympus BX43, Germany). Coupons were stained with Acridine Orange (0.01%; Fisher Scientific, United Kingdom) at 20 °C for 15 min. Biofilms were gently rinsed with sterile distilled water, air dried in the dark and observed at 100× magnification. Quantification of stained biofilms covering the coupons surfaces was performed by Python image processor software (Version 3.3.4., Python).

2.4.3. Scanning electron microscopy

Biofilms developed under the different flow conditions were also visualized using the scanning electron microscopy facility of the Advanced Characterization Platform of the Chevreul Institute (SEM; model JSM-7800FLV, JEOL, Japan). Biofilms developed on the SS coupons were fixed in Cacodylate buffer (sodium cacodylate trihydrate; 0.1 M, pH 7) prepared with 2% glutaraldehyde for 4 h at 4 °C. Biofilms were then dehydrated in increasing concentrations of ethanol, starting with 50%, followed by 75% and 90%, and finally with absolute ethanol with an exposure for 10 min in all cases. Subsequently, samples underwent a critical point drying and were sputter-coated with carbon prior to SEM observation. Quantification of stained biofilms covering the coupons surfaces was performed by Python image processor software (Version 3.3.4., Python).

2.5. Antibiofilm assays using monolayer and layer-by-layer thymol nanocapsules

2.5.1. Nanocapsules formation and size determination

Monolayer (ML) and layer-by-layer (LBL) nanocapsules encapsulating THY were prepared using the spray-drying technique. The ML nanocapsules were developed using MD as carrier material and CAS as emulsifier. For the LBL nanocapsules, LMP was added to the MD as a second carrier material. For the formation of capsules, primary emulsions were first prepared by a complete hydration of CAS in distilled water. Weighted amounts of THY were then added and the mixture was homogenized for 5 min at 20 000 rpm using an Ultra Turrax PT 4000 homogenizer (Polytron, Kinematica, Switzerland), then microfluidized at 500 bar using an LM20 Microfluidizer (Microfluidics Co., MA, USA). Subsequently, carrier MD solutions (50% w/v) (for both ML and LBL nanocapsules) and LMP solutions (2.5% w/v) (only for the LBL nanocapsules), were added to the emulsions. pH of the final solutions was adjusted to 3 by adding HCl (0.1 or 1.0 M) or NaOH (0.1 or 1.0 M) before the spray-drying process. The final composition of ML emulsions was: 20.0% MD, 0.5% CAS and 1.0% THY, and that of LBL emulsions was: 20.0% MD, 0.5% CAS, 1.0% THY, and 0.5% LMP. Emulsions were then injected into the nozzle of a mini spray-dryer (Büchi B-290, Switzerland) and the operating conditions were set as follow: 3.2 bar for the air pressure, 180 °C inlet air temperature, 80 °C outlet air temperature, and 0.5 L h^{-1} feed flow rate. Collected particles were stored at 4 °C in sealed containers until further analysis.

The size of the emulsions was measured using a Zetasizer Nano ZS90 (Malvern Instruments, UK) by suspending particles in imidazole-acetate buffer at pH 3 and performing the measurements in triplicate.

2.5.2. Minimal inhibitory concentration determination

The minimal inhibitory concentrations (MIC) of the ML and LBL THY nanocapsules were determined using the 96 wells microtiter plate assay. Briefly, 100 μL of *S.* Enteritidis bacterial suspension (10^6 CFU mL^{-1}) were added to 100 μL of Müller-Hinton Broth (MHB; Biokar Diagnostics, Pantin, France) in the microtiter plate wells. Subsequently, 100 μL of serial two-fold dilutions of the prepared capsules solutions were added to obtain final concentrations ranging from 0.156 to 5 mg mL^{-1}. This was performed by adding 100 μL of 5 mg mL^{-1} capsules solution to the first well, mixing well and then transferring 100 μL from the first well to the second well and so on, to obtain a final concentration of 0.156 mg mL^{-1} in the last well. MHB was used alone as a negative control, while for the positive control bacterial suspensions were added. The optical density at 600 nm (OD_{600}) was measured for 24 h in the incubated Bioscreen C (Labsystems, Helsinki, Finland) at 37 °C. The lowest concentrations that inhibited the visible growth of bacteria were determined as the MIC values. Three tests were performed independently.

2.5.3. Nanocapsules disinfection assays

To investigate the antibiofilm activity of ML and LBL THY nanocapsules against *S.* Enteritidis biofilms, the antimicrobial solutions were prepared in TS broth according to their ½ MIC values. A mixture of ML and LBL nanocapsules was also prepared to determine their combined effect on *S.* Enteritidis biofilms. Disinfection assays were performed on biofilms developed under the highest flow conditions of 0.087 cm s^{-1} in the pipeline system. After biofilm, formation, coupons were rinsed with PPB solution to remove loosely attached cells. ML capsules, LBL capsules and the mixture of both types of capsules solutions were then circulated peristaltically into the pipelines for 0.5 h, 2 h and 5 h. After the different exposure time, a neutralizing solution prepared by combining TS broth (9.5 g L^{-1}), Saponin (30 g L^{-1}), Tween 80 (30 g L^{-1}), L-Histidine (1 g L^{-1}), Sodium Thiosulphate (5 g L^{-1}), and Lecithin (30 g L^{-1}) was pumped for 10 min to stop the effect of the antimicrobial solutions. Rinsing with PPB solution was then performed. Coupons were removed from the three pipes of the set-up, soaked into 20 mL of TS broth, disrupted and quantified as previously described. Results were expressed as log CFU cm^{-2}. For each exposure time and treatment, three independent experiments were performed.

2.5.4. LIVE/DEAD epifluorescence microscopy observations

To assess the viability of *S.* Enteritidis biofilms and the extent of damage induced to their cell membranes, live and dead staining experiment was carried out. According to the LIVE/DEAD® BacLight kit (Invitrogen Molecular Probes, USA) instructions, biofilms exposed to the different treatments were stained for 15 min in the dark with SYTO-9 and propidium iodide. Then, coupons were thoroughly rinsed with distilled water and air dried in the dark. Epifluorescence microscopic observations were carried out at a 100× magnification.

2.5.5. Visualization of biofilms morphological alterations by scanning electron microscopy

Morphological alterations to recovered biofilm cells developed under the highest flow conditions were observed using SEM after exposure to a mixture of ML and LBL THY nanocapsules for 0.5 h, 2 h and 5 h. Recovered bacterial suspensions from coupons were diluted in TS broth. Then, 1 mL of the diluted suspension was filter sterilized using a 0.2 μm polycarbonate membrane filter (Schleicher & Schuell, Dassel, Germany) and fixed for 4 h in Cacodylate buffer with 2% glutaraldehyde at 4 °C. Filters were then dehydrated in increasing concentrations of ethanol, critical point dried, sputter-coated with carbon and observed under the SEM.

2.6. Statistical analysis

Three repetitions were carried out for the quantitative analysis of biofilm biomass. Data were statistically analyzed using the Matplotlib software (Version 3.3.4., Python). Analysis of Variance (ANOVA) followed by Tukey's test were performed. The statistical significance was set at $p < 0.05$.

3. Results and discussion

3.1. Biofilms formation under different dynamic conditions

3.1.1. Enumeration

Despite having a great influence on bacterial adhesion and subsequent biofilm formation, the effect of hydrodynamic conditions has been often neglected [21]. Therefore, experiments were performed to better understand how biofilm formation is influenced in response to fluid

flows as previous studies have shown that biofilms biomass, cell density and matrix production are greatly affected by the applied fluid conditions [22,23]. *S.* Enteritidis biofilm counts were assessed after 24 h incubation under three different flow conditions that simulate some of the real dynamic conditions encountered in the food industry (Fig. 2). *S.* Enteritidis biomass adhered to the SS coupons displayed significant differences between the three different flow conditions ($p < 0.05$). The mean counts reported were 5.96, 6.28 and 6.80 log CFU cm^{-2} under 0.006 cm s^{-1}, 0.045 cm s^{-1} and 0.087 cm s^{-1} flow velocities, respectively. Biofilm formation under the highest flow velocity of 0.087 cm s^{-1}, produced up to 12.4% greater biofilm biomass as compared to the lower flow rates. Previous studies have also shown similar trends with an enhanced biofilm development at higher flow conditions [24–26]. These results could be ascribed to the higher fluid flow that provides a greater continuous transport of nutrients and oxygen to coupons surfaces and to the inner parts of biofilms that subsequently promote biofilms growth [23,27]. The effect of greater nutrients availability under higher hydrodynamic conditions was confirmed by Ref. [28] who reported a favored *Escherichia coli* biofilm growth with higher amounts of nutrients. Similarly [24], showed an enhanced formation of *Thalassospira* biofilms at higher nutrient concentration. By contrast, the lower flow conditions that limit nutrient transport slowed down biofilm formation. Moreover, a higher flow of fluids was shown to facilitate bacterial communication efforts as the quorum sensing, and environment sensing as chemotaxis which promote biofilm formation [9]. Fluid dynamics may also help to deliver bacterial cells near surfaces with an assistance provided from bacterial appendages to help in the adhesion process, and may increase the production of extrapolymeric substances (EPS) that strengthen the biofilm matrix [9,29]. For instance Ref. [29], reported a simulated production of EPS with a subsequent enhancement in *Staphylococcus aureus* biofilm formation at higher flow conditions. Higher shear stress was additionally found to improve oxygenation and increase the expression of molecules involved in signal transduction, favoring thus biofilm development [21]. As an example [30], reported at higher shear stress an increased intracellular level of *cyclic-di-GMP* signals promoting biofilm formation. The high biofilm biomass reported at 0.087 cm s^{-1} fluid velocity, confirms that biofilms development and accumulation were sufficient enough to overcome the erosion induced by the highest flow applied [23]. These results corroborate previous findings where different biofilms had the highest cell density, biomass and extracellular polysaccharide and protein contents at the highest shear stress applied [22,31–33]. However, it should be pointed out that a reverse trend of biofilms formation could be observed with increased flow rates exceeding the highest flow rate tested. Higher flow rates could be accompanied by even more hydrodynamic forces that can slough of biofilms from the substratum or can lead to a non-attachment of biofilms due to the high shear forces imposed that could be above the critical levels for biofilms attachment [9,34–36].

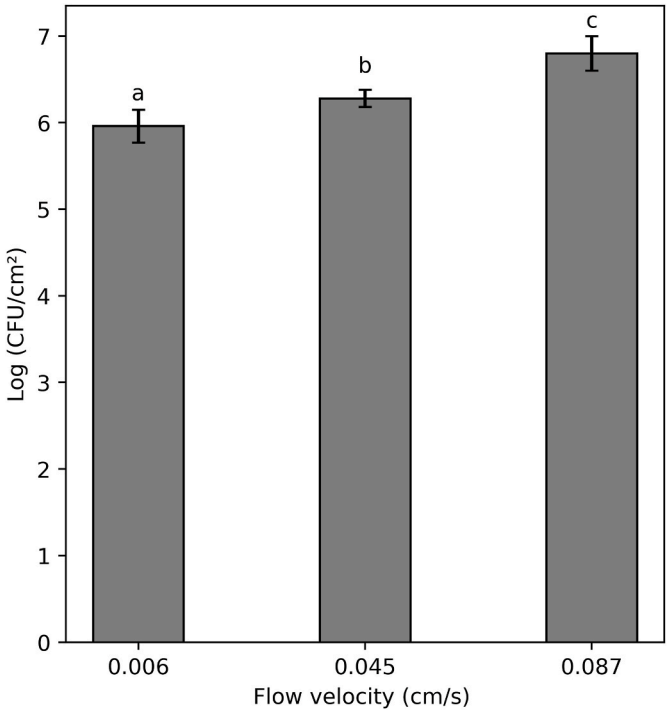

Fig. 2. S. Enteritidis biofilm quantification under different dynamic conditions. Data are expressed as mean log CFU cm^{-2} ± Standard Deviation (S.D.) of three independent experiments performed in triplicate. Significant ($p < 0.05$) results are indicated with different letters (a,b,c).

3.1.2. *Microscopic observations of the structure and spatial distribution of biofilms developed under different flows*

Biofilms structure and morphology could be highly affected by the surrounding flow conditions, and particularly, the local hydrodynamic forces that act on the biofilm-fluid interface [37,38]. Therefore, to further investigate the effect of different flow conditions on the structures and spatial distributions of biofilms, epifluorescence microscopy and SEM observations were performed (Fig. 3). After staining with Acridine Orange, the spatial and structural distribution of biofilms were clearly different between the different flow rates. An evident covered structure of biofilms was commonly observed under the epifluorescence microscopy. Denser, thicker and more abundant cell clusters covering 98.48% of coupon's surface were displayed for biofilms developed under the highest flow velocity of 0.087 cm s^{-1} in Fig. 3. A.3. Moreover, the presence of secreted EPS may be indicated by the presence of some diffused staining in Fig. 3. A.3. [29]; reported similar results with a higher secretion of EPS in *S. aureus* biofilms developed at higher flow rates. However, for biofilms formed under lower flow conditions, more separation occurred between cell clusters and some areas of the coupons were only covered with relatively small microcolonies or even single cells as shown in Fig. 3. A.1 and 3.A.2. Lower flow conditions of 0.006 cm s^{-1} displayed fewer aggregated clusters on the surface. Only 27.66% and 55.38% of the coupons surfaces were covered with biofilms at 0.006 cm s^{-1} and 0.045 cm s^{-1}, respectively. SEM images revealed similar results compared to the epifluorescence microscopy with dense extensive biofilm structures produced under the highest flow conditions in Fig. 3. B.3. The multilayer biofilm structures were embedded within a strand-like extracellular polymeric matrix and were characterized by thick, three-dimensional clusters that covered 99.32% of coupons surfaces [33]. corroborated similar results showing under the SEM, greater amounts of *Pseudomonas fluorescens* biofilms covering the whole stainless steel surfaces under the highest flow rates. Moreover [13], revealed a multilayered compact *Candida* biofilm structure with a higher quantity of produced EPS under dynamic conditions as compared to static ones. Conversely, biofilms grown under lower dynamic conditions of 0.006 cm s^{-1} and 0.045 cm s^{-1} displayed reduced biofilm bulk with 35.29% and 57.01% covered surfaces, respectively (Fig. 3. B.1 and 3.B.2). At reduced flow rates, more spread biofilm clusters were noticed with fewer bacterial cells. These microscopic observations confirm the previous enumeration findings highlighting the boosted formation of biofilms under higher flow conditions.

3.2. *Effect of thymol nanocapsules on biofilms developed under the highest flow conditions*

3.2.1. *Quantitative assessment of the antibiofilm activity by enumerating biofilm cells*

Previous studies highlighted the potent antibiofilm activity of encapsulated EO components [39–41]. Therefore in the present study, we focused on the potential use of THY ML and LBL nanocapsules to ensure an effective control of *S.* Enteritidis biofilms over time. The

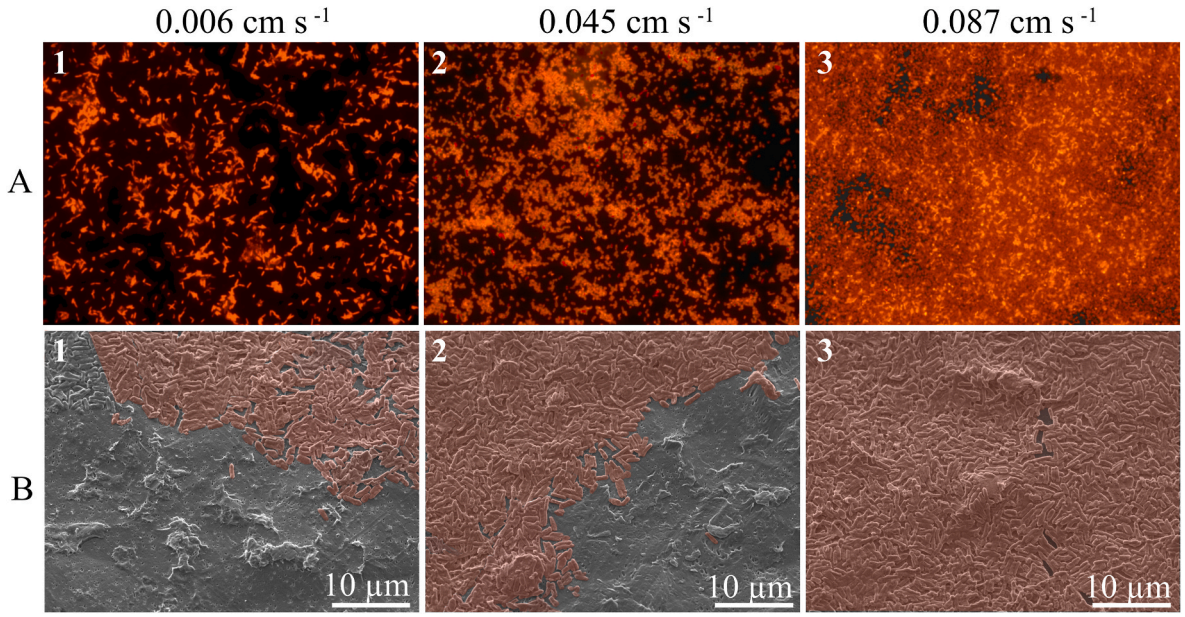

Fig. 3. (A) Epifluorescence microscopic observations of S. Enteritidis biofilms developed under different flow conditions: 3)A)1) 0.006 cm s^{-1}, 3)A)2) 0.045 cm s^{-1}, 3)A)3) 0.087 cm s^{-1}; and Fig. 3 (B) representing scanning electron microscopic observations of S. Enteritidis biofilms developed under different flow conditions: 3)B) 1) 0.006 cm s^{-1}, 3)B)2) 0.045 cm s^{-1}, 3)B)3) 0.087 cm s^{-1}.

average sizes of the developed ML and LBL THY nanocapsules were 159.2 nm and 283.6 nm, respectively. The bigger size of the LBL nanocapsules is probably due to the additional LMP layer added that increases the viscosity and subsequently the size of the LBL nanocapsules [42].

It is established that microorganisms in a biofilm state account for around 80% of microbial illnesses including foodborne diseases [11]. Therefore, efficient cleaning and disinfection methods should be adopted to control biofilm formation and guarantee food safety in food processing plants. The ability of ML-THY and LBL-THY nanocapsules to inhibit the planktonic growth of *S*. Enteritidis was assessed by measuring the MIC values. MIC displayed for both ML-THY and LBL-THY nanocapsules were 0.62 mg mL^{-1}. Similar MIC values for encapsulated THY were corroborated by Ref. [43] against *Salmonella*. The potential antibiofilm activity of nanocapsules was then assessed against *S*. Enteritidis biofilms developed under the highest flow velocity of 0.087 cm s^{-1}, that resulted in the highest biofilm biomass per coupon area of 6.16 cm^2. Fig. 4 represents the number of culturable bacteria as mean log CFU cm^{-2} after exposure to the different antimicrobial solutions prepared at

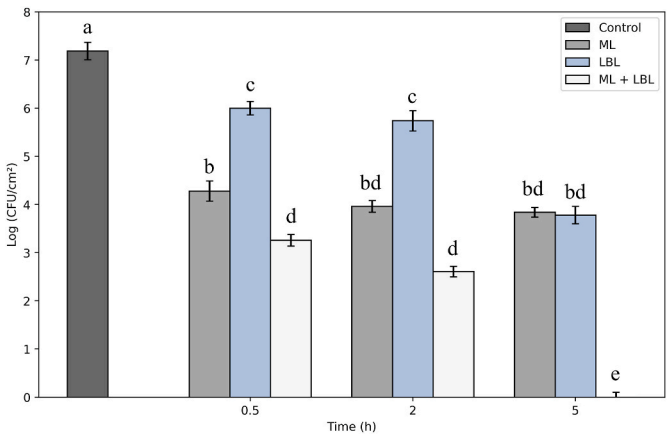

Fig. 4. Mean log CFU cm^{-2} of S. Enteritidis biofilms after exposure to ML and LBL nanocapsules at different exposure times. Different letters indicate significant ($p < 0.05$) differences.

½ MIC. ½ MIC values of nanocapsules were chosen for the treatments as they were the lowest concentrations tested with an efficient inhibitory effect (data not shown). ML nanocapsules induced biomass reductions of 2.9, 3.2, and 3.4 log after 0.5 h, 2 h and 5 h, respectively. During the first 0.5 h, ML capsules reduced significantly bacterial biofilms ($p < 0.05$). Whereas, after 2 h, no more significant additional biofilm reductions were displayed. These results demonstrate that most of the encapsulated THY was released from the ML nanocapsules during the first 2 h as no more significant antibiofilm activity was observed subsequently. Whereas after exposure to the LBL nanocapsules, biomass reductions of 1.2 and 1.5 log, were achieved after 0.5 h and 2 h, respectively. During the first 2 h, a diminished antibiofilm activity was observed due to the lower amounts of THY diffused out of the LBL nanocapsules. The retarded diffusion could be mainly attributed to the presence of LMP as an additional second droplet interfacial layer that provides a higher viscosity and thickness for the LBL nanocapsules retarding thus the diffusion of THY with a subsequent reduced antibiofilm effectiveness [44]. Whereas, after a prolonged exposure time for 5 h to the LBL nanocapsules, significant biomass reduction of 3.4 log was measured ($p < 0.05$). This gives evidence that THY needed more time to be diffused out of the LBL nanocapsules provoking thereby a sustained decrease of biofilms counts from the SS coupons over time. The combined effect of ML and LBL nanocapsules was additionally investigated on the removal of biofilms and it resulted in significant biomass reductions of 3.9 and 4.6 log after 0.5 h and 2 h, respectively ($p < 0.05$). This confirms that disinfection with a combination of the two types of capsules could enhance the activity of individually used capsules against biofilms developed under dynamic conditions. The promoted activity could be attributed to the combined effect of the terpenes released quickly from the ML capsules and the terpenes released from the LBL capsules even if in lower amounts, during the first 2 h. Furthermore, after 5 h, the combined treatment of ML and LBL nanocapsules presented an inhibitory effect with 99.99% eradication of biofilms. The prolonged antibiofilm activity over 5 h, could be mainly attributed to the LBL nanocapsules that released THY progressively and in a controlled manner. Whereas, the activity of the ML nanocapsules is considered as constant after 2 h, as already most of the encapsulated terpenes were released during the first 2 h. This prolonged antibiofilm activity over time, ensures a sustained protection of closed surfaces as pipelines and

tanks from bacterial contaminations and prevents the regrowth of residual surviving bacteria especially during the non-operating hours. The combination of capsules highlighted thus the potential use of ML nanocapsules for an initial immediate disinfection of surfaces due to the fast release of THY, and the LBL nanocapsules to remove residual bacterial cells that have not been eliminated previously while ensuring a long-term disinfection and protection of surfaces from microbial contaminations. Moreover, it should be noted that the hydrodynamic forces induced by the flow of the antimicrobial solutions in the pipelines, could promote the penetration of antimicrobials into the deep layers of biofilms sloughing of more easily attached biofilms from surfaces [9,27].

3.2.2. *Qualitative assessment of antibiofilm activity of thymol nanocapsules*

3.2.2.1. Viability and membrane damage of biofilm cells. After different exposure time to the ML, LBL and a mixture of both types of nanocapsules, the viability of *S*. Enteritis biofilms was observed under the epifluorescence microscopy and the results are displayed in Fig. 5. Live bacterial cells are stained with green by SYTO-9, while bacterial cells with damaged membranes are stained with red by propidium iodide. The results are consistent with the previous quantitative antibiofilm assessment. Control untreated bacterial cells exhibited a dense viable biofilm structure predominantly of live bacteria (green cells) at 0.5 h, 2 h and 5 h. While, after exposure to ML and LBL nanocapsules, there was an obvious decrease in green viable bacteria and an increase in red dead bacterial cells according to the different treatment types and exposure times. ML nanocapsules disrupted biofilms structure and induced membranes damage (marked by a red color) during the first 0.5 h mainly. While for the rest of the exposure time, no more remarkable membrane damage was displayed by the ML nanocapsules as there was no obvious increase in red coloration. This could be explained by the fact that ML nanocapsules provoked their main antibiofilm activity during the first 0.5 h, due to the initial burst release of THY. For the LBL nanocapsules, after 0.5 h and 2 h of treatment, green color dominated indicating that most of the cells remained viable as a retarded diffusion of THY occurred during the first 2 h. Whereas, after 5 h relatively more red cells with damaged bacterial membranes were observed. This is probably due to the additional time needed for the diffusion of THY out of the capsules and their subsequent antibiofilm activity. At the end, it can be also confirmed from the microscopic images that a combination of ML and LBL THY treatment for 5 h, achieved a total damage to biofilm cell membranes with dead red cells covering all the coupons surface. These results are similar to previous studies showing by microscopic observations the significant ability of encapsulated EOs components to penetrate into the deep layers of biofilms provoking bacterial cell damage and death [14,45,46].

3.2.2.2. Morphological alterations of biofilm cells. SEM images were obtained to visualize the structural differences between recovered *S*. Enteritidis biofilm cells treated with ML and LBL THY nanocapsules and those which were untreated. The combined effect of the nanocapsules on biofilms developed under the highest flow conditions was observed under the SEM after 0.5 h, 2 h and 5 h of exposure. The morphological alterations induced to bacterial cells after the different treatments are displayed in Fig. 6. Control untreated cells showed normal rod-shaped morphologies with smooth surfaces. Whereas after the first 0.5 h exposure to the ML and LBL nanocapsules, few biofilms recovered cells displayed a complete collapsed structure. The remaining cells showed intact structures with evident strand-like extrapolymeric substances linking bacteria and represented by white arrows in Fig. 6B. After 2 h of

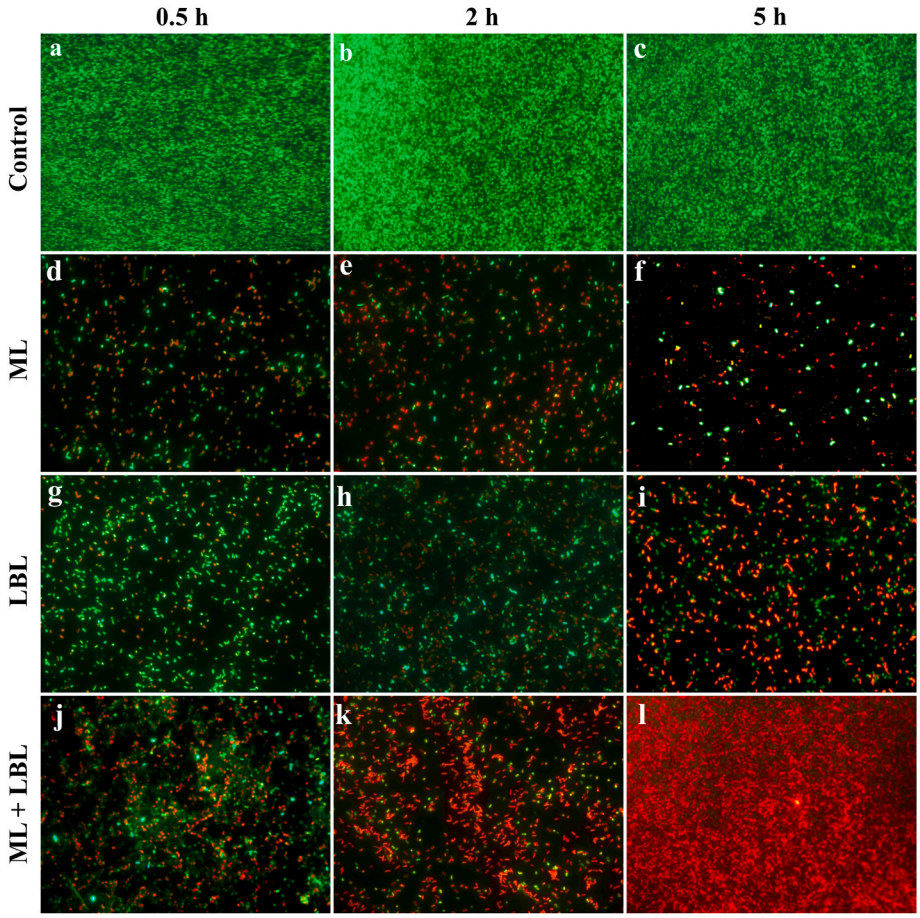

Fig. 5. Epifluorescence microscopic observations of the viability of S. Enteritids biofilms: control cells after a) 0.5 h, b) 2 h, and c) 5 h; exposed to ML nanocapsules after d) 0.5 h, e) 2 h, and f) 5 h; exposed to LBL nanocapsules after g) 0.5 h, h) 2 h, and i) 5 h; and exposed to a combined treatment of ML and LBL nanocapsules after j) 0.5 h, k) 2 h, and l) 5 h. Green cells stained with SYTO-9 represent viable bacteria with intact membranes whereas red cells stained with propidium iodide represent dead bacteria with damaged membranes. (For interpretation of the references to color in this figure legend, the reader is referred to the Web version of this article.)

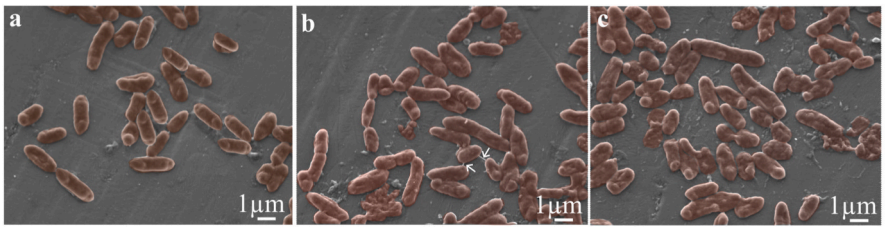

Fig. 6. Scanning electron microscopy images of recovered S. Enteritidis biofilm cells (a) control, and exposed to ML nanocapsules combined with LBL nanocapsules after exposure for (b) 0.5 h, (c) 2 h, and (d) 5 h.

exposure, remarkable additional deformation and shrinkage of most of the bacterial cells was observed. Moreover, after 5 h, almost all recovered biofilm cells were deformed, shrunken and wrinkled with holes in their structures, distinguishing them from the smooth and regular surfaces observed in control cells. Similar results were corroborated by Refs. [14,41] showing under the SEM, the great impact of encapsulated carvacrol and thymol on the morphology of bacterial cell membranes. The results suggest that an exposure to a combination of ML and LBL nanocapsules for a prolonged period of time is heavily involved in the destruction and death of bacterial cells. SEM micrographs confirm the diffusion of THY across biofilm structures and their direct effect on cell membranes which provokes a leakage of vital cell constituents with a subsequent deformation, shrinkage and death of bacterial cells. These observations are in agreement with the previously displayed results.

4. Conclusion

To mimic some of the real conditions encountered in food processing plants, *S*. Enteritidis biofilms were developed under different flow velocities in a pipeline system. Biofilm quantification was influenced by the different flow conditions as significantly greater biomass were displayed under the highest flows. At higher velocities, a greater replenishment of nutrients and substrates might occur which increases biofilms growth and development. Moreover, in this work we emphasized the potential use of ML and LBL THY nanocapsules to detach biofilms grown under dynamic conditions and to ensure a prolonged disinfection of food contact surfaces. Disinfection using a mixture of the two types of nanocapsules disrupted biofilms clusters, induced membrane damages and eradicated totally biofilms. ML nanocapsules ensured a primary efficient disinfection of surfaces, while LBL nanocapsules removed the remaining bacterial cells and displayed a prolonged protection of surfaces for up to 5 h, by releasing THY in a sustained and controlled manner over time. Future work is required for the implementation of essential oil terpene capsules in the food industries and the investigation of their combined effect with the hydrodynamic conditions to control biofilms and to ensure a long-term protection of surfaces. Also, further studies with much higher flow velocities are warranted to fully understand and elucidate the impact of different hydrodynamic conditions on biofilms growth as well as on their detachment.

Credit author statement

Jina Yammine: Design and conceptualization, Experiments, Data curation, Writing. **Adem Gharsallaoui:** Nanocapsules development, Writing- Reviewing and Editing. **Layal Karam and Ali Ismail:** Data curation, Writing- Reviewing and Editing. **Alexandre Fadel:** Scanning electron microscopy observations. **Nour-Eddine Chihib:** Conceptualization, Supervision, Writing- Reviewing and Editing. All authors read and approved the manuscript.

Funding

This work was supported by the Partenariat Hubert Curien PHC Cèdre program, France [42281SD].

Declaration of competing interest

The authors declare that they have no known competing financial interests or personal relationships that could have appeared to influence the work reported in this paper.

Data availability

Data will be made available on request.

Acknowledgments

The authors are grateful to Dr. Heni Dallagi and Laurent Wauquier for their valuable technical assistance. The Chevreul Institute is also thanked for its help in the development of this work through the ARCHI-CM project supported by the “Ministère de l’Enseignement Supérieur de la Recherche et de l’Innovation”, the region “Hauts-de-France”, the ERDF program of the European Union and the “Métropole Européenne de Lille.

References

[1] Ling N, Forsythe S, Wu Q, Ding Y, Zhang J, Zeng H. Insights into *Cronobacter sakazakii* biofilm formation and control strategies in the food industry. Engineering 2020;6:393–405. https://doi.org/10.1016/j.eng.2020.02.007.

[2] Pu H, Xu Y, Sun DW, Wei Q, Li X. Optical nanosensors for biofilm detection in the food industry: principles, applications and challenges. Crit Rev Food Sci Nutr 2021; 61:2107–24. https://doi.org/10.1080/10408398.2020.1808877.

[3] Byun KH, Na KW, Ashrafudoulla M, Choi MW, Han SH, Kang I, Park SH, Ha SD. Combination treatment of peroxyacetic acid or lactic acid with UV-C to control *Salmonella* Enteritidis biofilms on food contact surface and chicken skin. Food Microbiol 2022;102:103906. https://doi.org/10.1016/j.fm.2021.103906.

[4] Carrascosa C, Raheem D, Ramos F, Saraiva A, Raposo A. Microbial biofilms in the food industry - a comprehensive review. Int J Environ Res Publ Health 2021;18. https://doi.org/10.3390/ijerph18042014. 2014.

[5] Čabarkapa I, Čolović R, Đuragić O, Popović S, Kokić B, Milanov D, Pezo L. Antibiofilm activities of essential oils rich in carvacrol and thymol against *Salmonella* Enteritidis. Biofouling 2019;35:361–75. https://doi.org/10.1080/08927014.2019.1610169.

[6] Rather MA, Gupta K, Bardhan P, Borah M, Sarkar A, Eldiehy KSH, Bhuyan S, Mandal M. Microbial biofilm: a matter of grave concern for human health and food industry. J Basic Microbiol 2021;61:380–95. https://doi.org/10.1002/jobm.202000678.

[7] Rossi C, Chaves-López C, Serio A, Casaccia M, Maggio F, Paparella A. Effectiveness and mechanisms of essential oils for biofilm control on food-contact surfaces: an updated review. Crit Rev Food Sci Nutr 2022;62:2172–91. https://doi.org/10.1080/10408398.2020.1851169.

[8] Webber B, Oliveira A P de, Pottker ES, Daroit L, Levandowski R, Santos LR dos, Nascimento V P do, Rodrigues LB. *Salmonella* Enteritidis forms biofilm under low temperatures on different food industry surfaces. Ciência Rural 2019;49: e20181022. https://doi.org/10.1590/0103-8478cr20181022.

[9] Krsmanovic M, Biswas D, Ali H, Kumar A, Ghosh R, Dickerson AK. Hydrodynamics and surface properties influence biofilm proliferation. Adv Colloid Interface Sci 2021;288:102336. https://doi.org/10.1016/j.cis.2020.102336.

[10] Zhang H, Chen SP, Seck HL, Zhou W. Low-energy X-ray inactivation of *Salmonella* Enteritidis on shell eggs in mono-/co-culture biofilms with *Pseudomonas fluorescens*. Food Control 2021;123:107742. https://doi.org/10.1016/j.foodcont.2020.107742.

[11] Bénézech T, Faille C. Two-phase kinetics of biofilm removal during CIP. Respective roles of mechanical and chemical effects on the detachment of single cells vs cell

clusters from a *Pseudomonas fluorescens* biofilm. J Food Eng 2018;219:121–8. https://doi.org/10.1016/j.jfoodeng.2017.09.013.
[12] Ernst J, Klinger-Strobel M, Arnold K, Thamm J, Hartung A, Pletz MW, Makarewicz O, Fischer D. Polyester-based particles to overcome the obstacles of mucus and biofilms in the lung for tobramycin application under static and dynamic fluidic conditions. Eur J Pharm Biopharm 2018;131:120–9. https://doi.org/10.1016/j.ejpb.2018.07.025.
[13] Thein ZM, Samaranayake YH, Samaranayake LP. In vitro biofilm formation of *Candida albicans* and non-albicans *Candida* species under dynamic and anaerobic conditions. Arch Oral Biol 2007;52:761–7. https://doi.org/10.1016/j.archoralbio.2007.01.009.
[14] Mechmechani S, Gharsallaoui A, Fadel A, Omari KE, Khelissa S, Hamze M, Chihib NE. Microencapsulation of carvacrol as an efficient tool to fight *Pseudomonas aeruginosa* and *Enterococcus faecalis* biofilms. PLoS One 2022;17:e0270200. https://doi.org/10.1371/journal.pone.0270200.
[15] Bernal-Mercado AT, Juarez J, Valdez MA, Ayala-Zavala JF, Del-Toro-Sánchez CL, Encinas-Basurto D. Hydrophobic chitosan nanoparticles loaded with carvacrol against *Pseudomonas aeruginosa* biofilms. Molecules 2022;27:699. https://doi.org/10.3390/molecules27030699.
[16] Bisso Ndezo B, Tokam Kuaté CR, Dzoyem JP. Synergistic antibiofilm efficacy of thymol and piperine in combination with three aminoglycoside antibiotics against *Klebsiella pneumoniae* biofilms. Can J Infect Dis Med Microbiol 2021;2021:1–8. https://doi.org/10.1155/2021/7029944.
[17] Miranda-Cadena K, Marcos-Arias C, Mateo E, Aguirre-Urizar JM, Quindós G, Eraso E. In vitro activities of carvacrol, cinnamaldehyde and thymol against *Candida* biofilms. Biomed Pharmacother 2021;143:112218. https://doi.org/10.1016/j.biopha.2021.112218.
[18] Falleh H, Ben Jemaa M, Saada M, Ksouri R. Essential oils: a promising eco-friendly food preservative. Food Chem 2020;330:127268. https://doi.org/10.1016/j.foodchem.2020.127268.
[19] Singh S, Chaurasia SLBPK, Upendarrao G. A mini-review on the safety profile of essential oils. MOJ Biol Med 2022;7:33–6. https://doi.org/10.15406/mojbm.2022.07.00162.
[20] Nair A, Mallya R, Suvarna V, Khan TA, Momin M, Omri A. Nanoparticles—attractive carriers of antimicrobial essential oils. Antibiotics 2022;11:108. https://doi.org/10.3390/antibiotics11010108.
[21] Zheng S, Bawazir M, Dhall A, Kim HE, He L, Heo J, Hwang G. Implication of surface properties, bacterial motility, and hydrodynamic conditions on bacterial surface sensing and their initial adhesion. Front Bioeng Biotechnol 2021;9:643722. https://doi.org/10.3389/fbioe.2021.643722.
[22] Paul E, Ochoa JC, Pechaud Y, Liu Y, Liné A. Effect of shear stress and growth conditions on detachment and physical properties of biofilms. Water Res 2012;46:5499–508. https://doi.org/10.1016/j.watres.2012.07.029.
[23] Tsagkari E, Connelly S, Liu Z, McBride A, Sloan WT. The role of shear dynamics in biofilm formation. Npj Biofilms Microbiomes 2022;8:33. https://doi.org/10.1038/s41522-022-00300-4.
[24] Liu N, Skauge T, Landa-Marban D, Hovland B, Thorbjornsen B, Radu FA, Vik BF, Baumann T, Bodtker G. Microfluidic study of effects of flow velocity and nutrient concentration on biofilm accumulation and adhesive strength in the flowing and no-flowing microchannels. J Ind Microbiol Biotechnol 2019;46:855–68. https://doi.org/10.1007/s10295-019-02161-x.
[25] Thomen P, Robert J, Monmeyran A, Bitbol AF, Douarche C, Henry N. Bacterial biofilm under flow: first a physical struggle to stay, then a matter of breathing. PLoS One 2017;12:7e0175197. https://doi.org/10.1371/journal.pone.0175197.
[26] Zhu J, Wang M, Zhang H, Yang S, Song KY, Yin R, Zhang W. Effects of hydrophilicity, adhesion work, and fluid flow on biofilm formation of PDMS in microfluidic systems. ACS Appl Bio Mater 2020;3:8386–94. https://doi.org/10.1021/acsabm.0c00660.
[27] Tsai YP. Impact of flow velocity on the dynamic behaviour of biofilm bacteria. Biofouling 2005;21:267–77. https://doi.org/10.1080/08927010500398633.
[28] Teodosio JS, Simoes M, Melo LF, Mergulhao FJ. Flow cell hydrodynamics and their effects on *E. coli* biofilm formation under different nutrient conditions and turbulent flow. Biofouling 2011;27:1–11. https://doi.org/10.1080/08927014.2010.535206.
[29] Hou J, Veeregowda DH, van de Belt-Gritter B, Busscher HJ, van der Mei HC. Extracellular polymeric matrix production and relaxation under fluid shear and mechanical pressure in *Staphylococcus aureus* biofilms. Appl Environ Microbiol 2018;84:e01516–7. https://doi.org/10.1128/AEM.01516-17.
[30] Rodesney CA, Roman B, Dhamani N, Cooley BJ, Katira P, Touhami A, Gordon VD. Mechanosensing of shear by Pseudomonas aeruginosa leads to increased levels of the cyclic-di-GMP signal initiating biofilm development. Proc Natl Acad Sci USA 2017;114:5906–11. https://doi.org/10.1073/pnas.1703255114.
[31] Araujo PA, Malheiro J, Machado I, Mergulhao F, Melo L, Simoes M. Influence of flow velocity on the characteristics of *Pseudomonas fluorescens* biofilms. J Environ Eng 2016;142:04016031. https://doi.org/10.1061/(ASCE)EE.1943-7870.
[32] Lemos M, Mergulhão F, Melo L, Simões M. The effect of shear stress on the formation and removal of Bacillus cereus biofilms. Food Bioprod Process 2015;93:242–8. https://doi.org/10.1016/j.watres.2012.07.029.
[33] Simoes M, Pereira MO, Sillankorva S, Azeredo J, Vieira MJ. The effect of hydrodynamic conditions on the phenotype of *Pseudomonas fluorescens* biofilms. Biofouling 2007;23:249–58. https://doi.org/10.1080/08927010701368476.
[34] Cowle MW, Webster G, Babatunde AO, Bockelmann-Evans BN, Weightman AJ. Impact of flow hydrodynamics and pipe material properties on biofilm development within drinking water systems. Environ Technol 2020;41:3732–44. https://doi.org/10.1080/09593330.2019.1619844.
[35] Gomes LC, Mergulhão FJ. A selection of platforms to evaluate surface adhesion and biofilm formation in controlled hydrodynamic conditions. Microorganisms 2021;9:1993. https://doi.org/10.3390/microorganisms9091993.
[36] Zhang W, Sileika T, Packman AI. Effects of fluid flow conditions on interactions between species in biofilms. FEMS (Fed Eur Microbiol Soc) Microbiol Ecol 2013;84:344–54. https://doi.org/10.1111/1574-6941.12066.
[37] Kostenko V, Salek MM, Sattari P, Martinuzzi RJ. Staphylococcus aureus biofilm formation and tolerance to antibiotics in response to oscillatory shear stresses of physiological levels. FEMS Immunol Med Microbiol 2010;59:421–31. https://doi.org/10.1111/j.1574-695X.2010.00694.x.
[38] Paris T, Skali-Lami S, Block JC. Effect of wall shear rate on biofilm deposition and grazing in drinking water flow chambers. Biotechnol Bioeng 2007;97:1550–61.
[39] Heckler C, Silva CMM, Cacciatore FA, Daroit DJ, Da Silva Malheiros P. Thymol and carvacrol in nanoliposomes: characterization and a comparison with free counterparts against planktonic and glass-adhered. Salmonella. LWT 2020;127:109382. https://doi.org/10.1016/j.lwt.2020.109382.
[40] Mechmechani S, Khelissa S, Gharsallaoui A, Omari KE, Hamze M, Chihib NE. Hurdle technology using encapsulated enzymes and essential oils to fight bacterial biofilms. Appl Microbiol Biotechnol 2022;106:2311–35. https://doi.org/10.1007/s00253-022-11875-5.
[41] Yammine J, Gharsallaoui A, Fadel A, Mechmechani S, Karam L, Ismail A, et al. Enhanced antimicrobial, antibiofilm and ecotoxic activities of nanoencapsulated carvacrol and thymol as compared to their free counterparts. Food Control 2023;143:109317. https://doi.org/10.1016/j.foodcont.2022.109317.
[42] Kord Heydari M, Assadpour E, Jafari SM, Javadian H. Encapsulation of rose essential oil using whey protein concentrate-pectin nanocomplxes: optimization of the effective parameters. Food Chem 2021;356:129731. https://doi.org/10.1016/j.foodchem.2021.129731.
[43] Engel JB, Heckler C, Tondo EC, Daroit DJ, da Silva Malheiros P. Antimicrobial activity of free and liposome-encapsulated thymol and carvacrol against Salmonella and Staphylococcus aureus adhered to stainless steel. Int J Food Microbiol 2017;252:18–23. https://doi.org/10.1016/j.ijfoodmicro.2017.04.003.
[44] Das S, Singh VK, Chaudhari AK, Deepika, Dwivedy AK, Dubey NK. Co-encapsulation of Pimpinella anisum and Coriandrum sativum essential oils based synergistic formulation through binary mixture: physico-chemical characterization, appraisal of antifungal mechanism of action, and application as natural food preservative. Pestic Biochem Physiol 2022;184:105066. https://doi.org/10.1016/j.pestbp.2022.105066.
[45] De Alteriis E, Maione A, Falanga A, Bellavita R, Galdiero S, Albarano L, Salvatore MM, Galdiero E, Guida M. Activity of free and liposome-encapsulated essential oil from Lavandula angustifolia against persister-derived biofilm of *Candida auris*. Antibiotics 2021;11:26. https://doi.org/10.3390/antibiotics11010026.
[46] Duncan B, Li X, Landis RF, Kim ST, Gupta A, Wang LS, Ramanathan R, Tang R, Boerth J, Rotello V. Nanoparticle-stabilized capsules for the treatment of bacterial biofilms. ACS Nano 2015;9:7775–82. https://doi.org/10.1021/acsnano.5b01696.